J. Fluid Mech. (1997), *vol.* 344, *pp.* 291–316. Printed in the United Kingdom

Natural convection during solidification of an alloy from above with application to the evolution of sea ice

By J. S. WETTLAUFER[1], M. GRAE WORSTER[2] AND HERBERT E. HUPPERT[2]

[1]Applied Physics Laboratory and Department of Physics, University of Washington, Box 355640, Seattle, WA 98105, USA
e-mail: wett@aph.washington.edu

[2]Institute of Theoretical Geophysics, Department of Applied Mathematics and Theoretical Physics, University of Cambridge, Silver Street, Cambridge CB3 9EW, UK
e-mail: grae@esc.cam.ac.uk; heh1@esc.cam.ac.uk

(Received 24 July and in revised form 27 March 1997)

We describe a series of laboratory experiments in which aqueous salt solutions were cooled and solidified from above. These solutions serve as model systems of metallic castings, magma chambers and sea ice. As the solutions freeze they form a matrix of ice crystals and interstitial brine, called a mushy layer. The brine initially remains confined to the mushy layer. Convection of brine from the interior of the mushy layer begins abruptly once the depth of the layer exceeds a critical value. The principal path for brine expelled from the mushy layer is through 'brine channels', vertical channels of essentially zero solid fraction, which are commonly observed in sea ice and metallic castings. By varying the initial and boundary conditions in the experiments, we have been able to determine the parameters controlling the critical depth of the mushy layer. The results are consistent with the hypothesis that brine expulsion is initially determined by a critical Rayleigh number for the mushy layer. The convection of salty fluid out of the mushy layer allows additional solidification within it, which increases the solid fraction. We present the first measurements of the temporal evolution of the solid fraction within a laboratory simulation of growing sea ice. We show how the additional growth of ice within the layer affects its rate of growth.

1. Introduction

The surface of the polar oceans undergoes an annual cycle during which the difference between the minimum and maximum ice coverage is 8×10^6 km^2 in the Arctic and 18×10^6 km^2 in the Antarctic. In the Arctic winter, one half of the surface heat flux to the atmosphere derives from latent heat release during solidification, accounting for one sixth of the radiative heat loss to space (Peixoto & Oort 1992). Thus freezing makes an important contribution to the atmospheric energy budget. In addition, the cooling and freezing of the polar oceans are important processes in the formation of deep ocean currents (Aagaard & Carmack 1994). Although these processes are included coarsely in models of atmospheric dynamics and ocean circulations, relatively little is known of the interactions between fluid dynamics and thermodynamics during young sea-ice formation.

Deformations of sea ice regularly create cracks, known as leads, which can be from a few metres to several kilometres in width. In the Arctic winter, the relatively warm ($-2\,^{\circ}$C) water in leads is exposed to the cold ($-30\,^{\circ}$C to $-60\,^{\circ}$C) air above it. A thin veneer of ice rapidly forms across an exposed lead. After one day's growth the layer of ice is about 10 cm deep, which is still thin compared with the surrounding ice, which is typically several metres thick. Recent field observations (Morison *et al.* 1993) show that the heat loss through leads can be up to 300 W m^{-2}, or fifteen times that from the surrounding ice. Therefore, although leads occupy less than 10% of the surface area, they can account for roughly half of the total oceanic heat loss. Furthermore, the brine flux emanating from leads is thought to control the large-scale thermohaline structure of the upper Arctic Ocean (Morison *et al.* 1993). Finally, the tremendous proportion of the deep ocean occupied by Antarctic Bottom Water is directly connected to sea-ice formation on continental shelves (Gill 1973). It is the initial formation of ice in leads and its growth during the first few days that provide the focus for the present study.

Early field observations of sea ice (Malmgren 1927) confirmed that, in bulk, it has a salinity that is much less than that of the ocean from which it formed. In addition, it was found that the bulk salinity of the ice first formed in leads is larger when the air temperature is colder. It is now known that brine channels form the main conduits through which such desalination occurs. Brine channels have been observed in previous field (Bennington 1963; Lake & Lewis 1970) and laboratory (Eide & Martin 1975) experiments. Here we uncover the mechanisms associated with their formation.

Although the primary motivation for this study is to understand the formation of sea ice, it forms part of a more general study of the dynamics of solidifying alloys or mixtures. Huppert & Worster (1985) described qualitatively the different dynamical possibilities that can occur in a two-component system depending on whether the mixture is solidified from below or from above and whether the component rejected by the growing solid causes the liquid to become more or less dense. In the case of sea ice, the liquid is cooled from above and the rejected salt causes the liquid to become more dense. Therefore, both the thermal and the compositional buoyancy have the potential to drive convection.

When alloys are solidified, the solid–liquid interface is typically unstable to morphological perturbations, and a mushy region is created in which the solid forms a porous medium whose interstices are filled with residual melt. The dynamics of mushy layers, in particular the propensity for natural convection of the interstitial melt to occur, depends crucially on their solid fraction, which varies both spatially and temporally as the layer evolves. The solid fraction controls many important physical properties in metallic castings and it exerts a major influence on the acoustic (Williams, Garrison & Mourad 1992), electromagnetic (Winebrenner *et al.* 1992) and mechanical (Weeks 1997) behaviour of sea ice. Our experiments provide the first measurements of the solid fraction of growing sea ice and how this fraction evolves in time.

The system we investigate here has many similarities to those in which alloys are cooled from below and release a light residual as they solidify. In particular, these systems have in common the possibility of compositionally driven convection of the interstitial melt and the formation of channels or 'chimneys'. Most experiments in this geometry have been conducted using aqueous solutions of ammonium chloride (NH_4Cl) (Copley *et al.* 1970, Huppert 1990; Chen & Chen 1991; Tait & Jaupart 1992; Hellawell, Sarazin & Steube 1993), which has a very steep liquidus. For this reason, it has not been possible to vary the experimental parameters very widely, especially not

the initial concentration of the solution. By contrast, in the experiments we describe here, in which ice is grown from aqueous solutions of sodium chloride (NaCl), the experimental parameters have been varied over a wide range, enabling a much fuller exploration of the conditions required for convection within the mushy layer.

In §2 we describe the experimental apparatus and procedure. The observations from a particular experiment are described in detail in §3. In §4 we summarize data from a suite of experiments in which the initial concentration of the liquid and the temperature of the cooled upper boundary were varied. This allows us to infer key features of the dynamical mechanisms controlling the growth of ice from aqueous salt solutions in §5. Finally, in §6, we draw conclusions from this study relating to the early formation and growth of sea ice.

2. Experimental apparatus and procedure

We conducted a series of experiments in which aqueous solutions of NaCl were cooled and solidified from above. The apparatus consisted of a Perspex tank, with walls 11 mm thick, of dimensions $20 \times 20 \times 37.6$ cm with a brass lid as depicted in figure 1. The lid had a double-spiral channel within it through which was pumped cooled ethylene glycol (anti-freeze). A thermistor, marked 'A', was embedded in the lid close to its contact with the liquid or mushy layer. The temperature of the coolant was continually adjusted in order to achieve and maintain the lid at a constant temperature. All the other walls of the tank were insulated with 5 cm thick expanded polystyrene and the whole apparatus was placed in a chamber with independent temperature control, thereby suppressing heat gains from the laboratory. The depth of the mushy layer was measured with a millimetre scale fixed to the side of the tank. Seven thermistors, marked 'B' to 'H', were placed at 1, 2, 4, 8, 12, 20 and 30 cm from the upper boundary, at least 5 cm away from any side wall. The tank was airtight and a tube led from a hole in its side near the base to allow for any expansion of the solution as it cooled and solidified. The tube led to a graduated burette so that the amount of expansion could be recorded as a function of time. This provided the primary measurement from which the volume of ice grown was determined.

Before an experiment began the solution in the tank was cooled to a uniform temperature of approximately $-2\,^{\circ}$C. This was the starting temperature for all the experiments except two in which the concentration of the solution was only 1 wt% or 2 wt% NaCl. In these cases, the initial temperature of the solution was set to within $1\,^{\circ}$C above the relevant liquidus temperature (figure 2). An experiment was started by allowing the pre-cooled refrigerant to circulate through the top plate. During the experiment, the thermistors were automatically monitored by a computer. Periodically, the depth of the mushy layer, the level of liquid in the burette and the concentration of samples withdrawn at 10 cm, 20 cm and 30 cm below the cooled plate were recorded simultaneously.

We report here on thirteen experiments with initial concentrations ranging from 1 to 14 wt% NaCl and top-plate temperatures ranging between $-10\,^{\circ}$C and $-20\,^{\circ}$C. The initial conditions of the various experiments are shown in figure 2.

3. Results from a particular experiment

Before describing the suite of experiments in generality, we present in detail the observations made and data collected from a particular experiment using an aqueous solution of 7 wt% NaCl. The initial temperature of the solution was $-1.84\,^{\circ}$C and

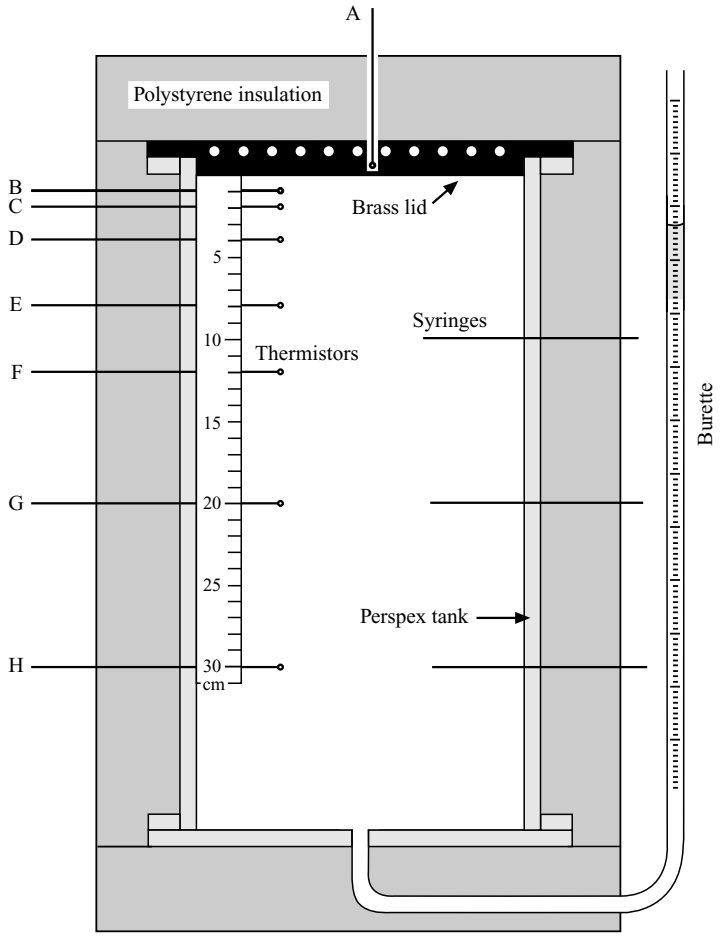

FIGURE 1. A schematic diagram of the Perspex tank with a brass lid, which contained the salt solution. The tank was housed in another cooled insulated chamber with independent temperature control in order to minimize heat transfer from the laboratory. Any expansion or contraction of the solution and container was accommodated by the graduated burette. The brass lid contained a spiral channel through which coolant was pumped. Temperatures were measured by thermistor beads and recorded automatically by computer. Samples of solution were withdrawn through syringes and their compositions were measured optically.

the temperature of the top boundary (the surface temperature) was maintained at $-20\,^{\circ}\mathrm{C}$. All the experiments were conducted in a similar way.

Vigorous thermal convection was observed at the start of the experiment, which weakened after a few minutes once solidification of ice on the top plate had commenced. The ice formed a uniform mushy layer having a nearly horizontal interface with the liquid below it. It was noticeable that the mushy layer comprised approximately vertical platelets of ice, characteristic of the structure of columnar sea ice in which the solid matrix is composed of pure ice platelets with randomly oriented horizontal c-axes (Weeks & Wettlaufer 1996; Wettlaufer 1997). Compositional convection in the form of thin streamers (figure 3*a*) was observed as salt was rejected by the growing ice. The compositional convection would have augmented the thermal convection which, though weaker than at the start, remains significant throughout the experiment. However, as we discuss in detail below, despite the appearance of

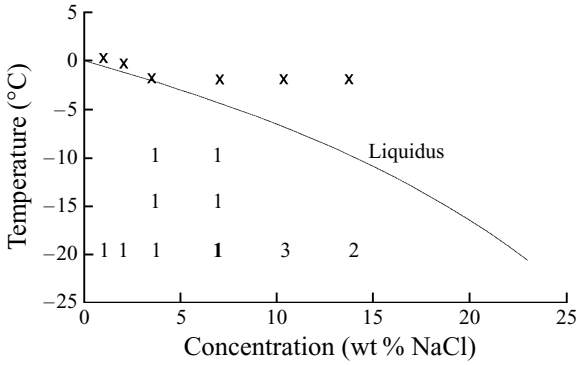

FIGURE 2. The liquidus curve for aqueous sodium chloride. The numbers indicate the number of experiments conducted with that initial concentration and temperature of the cooled lid of the apparatus. The crosses indicate the corresponding initial temperature of the liquid. The typical experiment discussed in §3, shown in bold, had an initial concentration of 7 wt% and the surface temperature was −20°C.

compositional convection, most of the rejected salt remained trapped within the interstices of the mushy layer at this stage of the experiment. The general appearance of the system did not change (except that the mushy layer became deeper) until about 12 hours from the start, when several larger plumes of brine became apparent (figure 3*b*). These plumes emanated from what have become known as 'chimneys' in the metallurgical community (figure 3*c*). The chimneys are vertical channels devoid of solid which form the principal route for convection of the interstitial liquid out of the mushy layer. They have been observed most clearly when aqueous solutions of ammonium chloride (NH_4Cl) have been cooled and crystallized from below (Copley *et al.* 1970; Huppert 1990; Chen & Chen 1991; Tait & Jaupart 1992; Hellawell *et al.* 1993) but see also Huppert & Hallworth (1993) and Worster & Kerr (1994). In the context of sea ice, the chimneys can be identified as brine channels. In our experiments, the brine channels were 1–2 mm in diameter.

It might have been anticipated that the convection responsible for channel formation would be so influenced by the anisotropy of the permeability of a medium composed of platelets that channels would not form at all or that they might be elongated in cross-section, aligned with the local platelets. However, looking end on to the channels (figure 3*c*), it is striking that their circular cross-section seems to be unaffected by the platelet structure of the ice crystals. The channels form no particular pattern in the horizontal and the spacing between them appears quite random, but on average they are approximately 1 cm apart. This is much closer (relative to the depth of the mushy layer, which was 20 cm when the photograph was taken) than the chimneys seen in ammonium-chloride mushy layers, whose spacing is comparable to the depth of the layer. This may be a consequence of the different morphologies of the solid phase in the two systems altering the form of fluid motion in the mushy layer. In the case of ice, the vertical platelets cause a strongly anisotropic permeability. The permeability is more nearly orthotropic, being horizontally isotropic but having a vertical permeability that is much greater than the horizontal permeability. This will inhibit lateral motions, which is consistent with the aspect ratio of the convective cells producing channels being small. A *post mortem* revealed that the brine channels extended the full depth of the mushy layer.

For the purposes of our subsequent discussion, the description will be in terms of

(*a*)

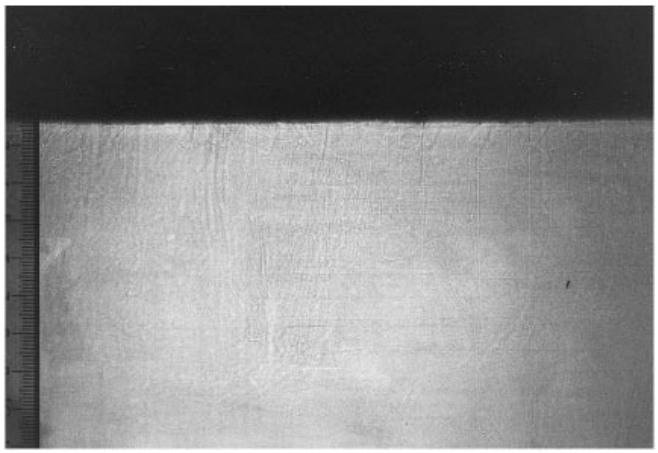

(*b*)

FIGURE 3. Photographs taken during an experiment in which an aqueous solution of sodium chloride (3.55 wt%) was cooled and solidified from above at a base-plate temperature of $T_B = -15°\mathrm{C}$. A centimetre scale is shown on the left. The black region at the top of the photographs in (*a*), (*b*), and (*d*) is the mushy layer. (*a*) Early in the experiment, when the mushy layer has a depth of 2.4 cm, weak interfacially driven compositional convection is evident in the form of very thin streamers. These emanate mainly from the interfacial region between the mushy layer and the liquid and do not carry a significant flux of salt (see figure 6). (*b*) Later in the experiment, when the depth of the mushy layer is about 11.5 cm, which is greater than the critical

(*c*)

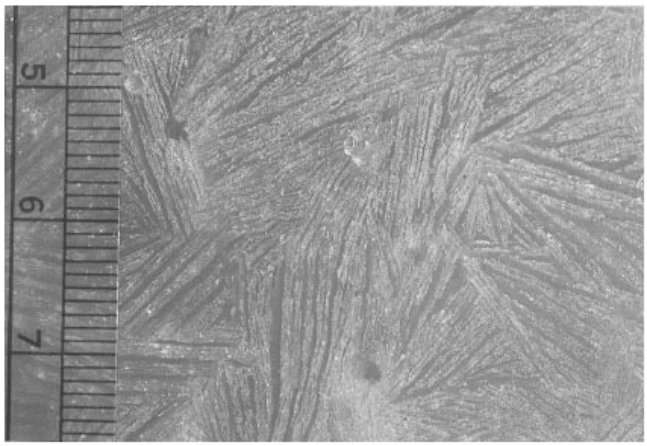

(*d*)

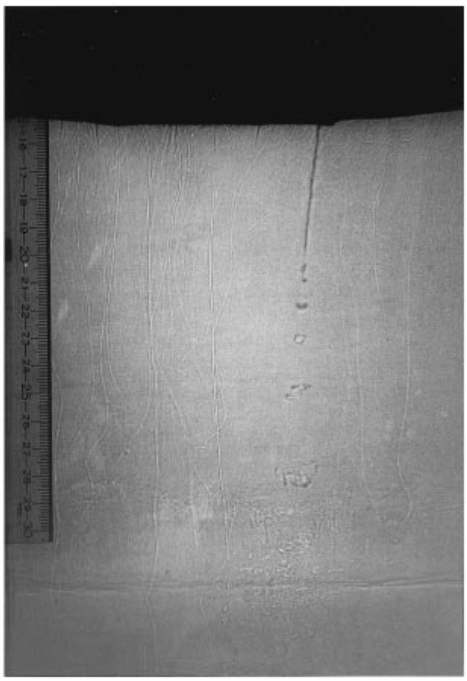

depth h_c (see figure 6), strong plumes of brine emanate from deep within the mushy layer and emerge from brine channels within the layer. These plumes carry a significant salt flux and distinguish 'internally driven' convection from 'interfacially driven' convection shown in (*a*) (see text). (*c*) A view perpendicular to the decanted interface parallel to the axis of a brine channel. (*d*) Double-diffusive layering at the base of the tank provides evidence that a stable salt stratification is achieved through a filling-box mechanism (Baines & Turner 1969) where it becomes warmed by heat through the sides of the tank. Because of the stable compositional stratification, it does not mix with the cooled convecting liquid above it (Thorpe *et al.* 1969).

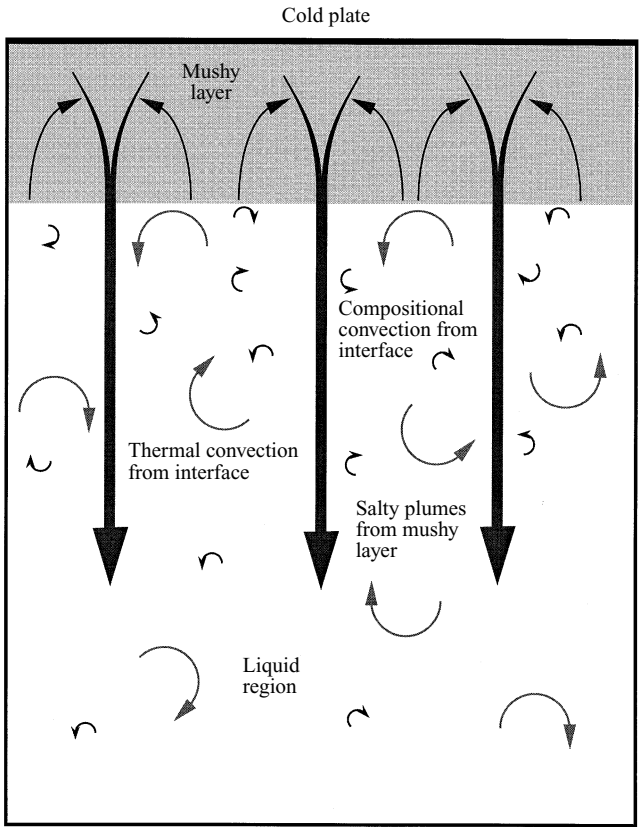

FIGURE 4. A schematic diagram indicating the three types of convection that occur in the experimental system. Both small-scale compositional convection (depicted by small round arrows) and large-scale thermal convection (depicted by larger round arrows) originate from the interfacial region between the mushy layer and the liquid region and keep the liquid well mixed. The initial small-scale compositional convection does not carry much salt and the concentration of the liquid region remains constant to within the resolution of our measurements. After some time into an experiment additional compostional convection (depicted by large vertical arrows) emerges in the form of plumes from the interior of the mushy layer and is replaced by a slow return flow of fresher liquid from below. This convection carries much more salt so, once it occurs, the composition of the liquid region evolves in time. It is likely that the plumes, which mix less well than the small-scale convection from the interface, are reponsible for setting up the weak compositional gradient at the base of the tank that allows double-diffusive layers to form there (see figure 3*d*).

just two types of convection, as illustrated in figure 4. Convection is driven in the liquid region as a result of the density difference between the liquid near the mush–liquid interface and the liquid in the fully liquid region. This density difference is due partly to a temperature difference and partly to a compositional difference. The latter would be predicted to be zero in a theory that assumed thermodynamic equilibrium at the mush–liquid interface and also assumed the interface to be planar. It is non-zero once either non-equilbrium effects are taken into account or it is appreciated that compositional convection can arise from the tips of the crystals in the neighbourhood of the interface, in other words that the 'interface' is a region of finite size (Worster & Kerr 1994). We shall refer to the thermal *and* compositional convection driven from the interfacial region as 'interfacially driven' convection. The second type of convection to which we shall refer is that emanating from the interior of the mushy

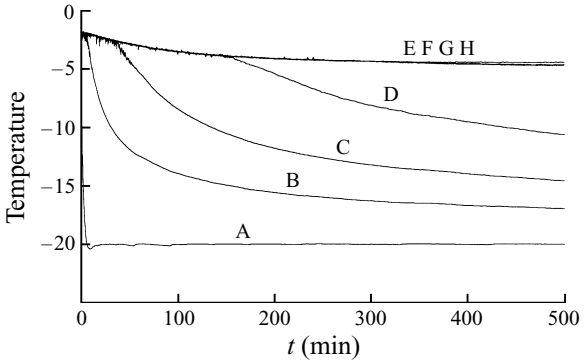

FIGURE 5. The temperatures recorded by the thermistors as function of time. Note that the thermistors all record the same temperature while they are in the liquid region but record lower temperatures once they are engulfed by the advancing mushy layer.

layer. We refer to this type of convection as 'internally driven' convection. It is driven primarily by compositional density gradients which dominate those caused by the thermal field within the mushy layer.

The primary data recorded from this experiment are shown in figures 5–9. In figure 5, the temperature traces from all eight thermistors are shown. It can be seen that the temperature of the cold upper boundary (thermistor A) dropped quickly to $-20\,^{\circ}\mathrm{C}$ and was constant thereafter. Apart from minor fluctuations, the other thermistors recorded the same (slowly decreasing) temperature while they were in the liquid region but the traces peel off to lower values as each thermistor became engulfed by the mushy layer. The temperature at the lowermost thermistor (H) increased slightly above the general temperature of the liquid region at late stages in an experiment. This may be due to dense saline fluid ponding at the base of the tank by the filling-box mechanism (Baines & Turner 1969) where it becomes warmed by heat from the laboratory. Although heated, it is too saline to mix with the cooled convecting liquid above it. Indeed, there is some evidence of compositional stratification near the base of the tank from the presence of double-diffusive layering there (figure 3*d*), probably caused by heat transfer through the sides of the tank acting on a stable compositional stratification (Thorpe, Hutt & Soulsby 1969).

In figure 6 we show the measured concentrations in the liquid region as functions of time (figure 6*a*) and of the depth of the mushy layer (figure 6*b*). The compositional stratification mentioned above was too weak to be resolved by the refractometer used to determine the concentration. So, to within our experimental error, the composition of the liquid region was uniform. It is clear that the concentration remained constant in time until after about 200 minutes, when the mushy layer was about 5 cm deep, as indicated by the hand-drawn curves in figure 6. In other words, essentially all the salt rejected by the growing ice initially remained trapped within the interstices of the mushy layer. This phase of the evolution corresponds to the form of compositional convection evident in figure 3(*a*). Our interpretation is that this weak convection originates from the mush–liquid interfacial region where the interstitial concentration is close to the far-field concentration in the liquid region. Only after the mushy layer had grown to some depth h_c, which we shall call the 'critical depth', was there a significant flux of brine out of the mushy layer into the liquid beneath. The increased brine flux appears to be associated with the form of convection shown in figure 3(*b*), in which plumes of dense salty fluid emerge from deep within the mushy layer. The

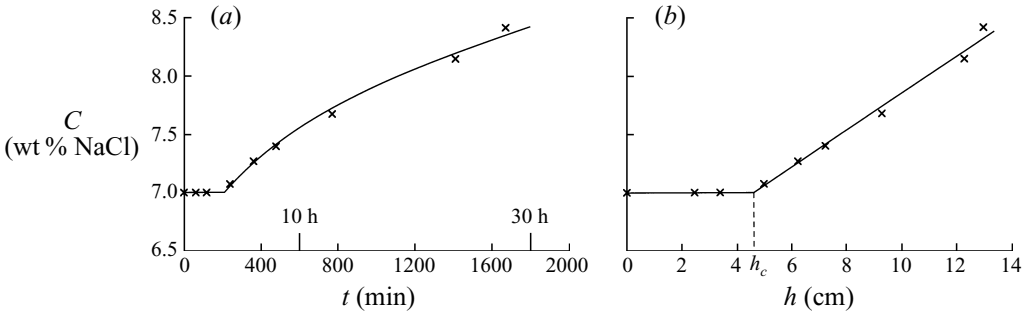

FIGURE 6. (*a*) The concentration of the liquid region and (*b*) the depth of the mushy layer as functions of time. The concentration intially remains constant indicating that the salt rejected by the growing ice remains trapped within the mushy layer. Once the depth of the mushy layer exceeds a critical value h_c, salt is convected out of the mushy layer and causes the concentration of the liquid region to increase. The solid curves are hand-drawn to fit the data.

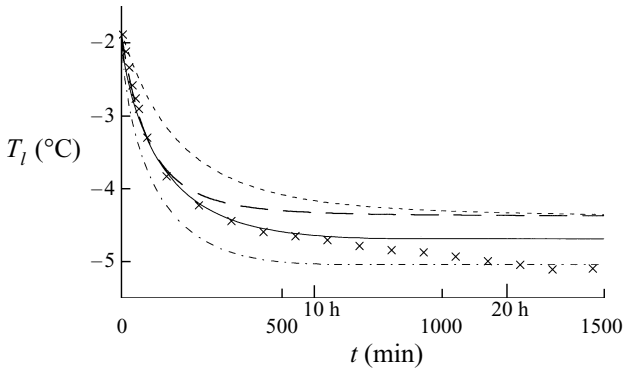

FIGURE 7. The temperature of the liquid region as a function of time. The crosses show the experimental data while the four curves show the predictions of a mathematical model with different values of the kinetic coefficient $\mathscr{G}$ and the heat-flux coefficient λ: – – – –, $\mathscr{G} = \infty$, $\lambda = 0.056$; — — —, $\mathscr{G} = \infty$, $\lambda = 0.12$; ——, $\mathscr{G} = 4 \times 10^{-4}$, $\lambda = 0.056$, – · – · – · –, $\mathscr{G} = 2.2 \times 10^{-4}$, $\lambda = 0.056$.

initiation of a significant brine flux from the mushy layer only after the mushy layer has achieved a certain depth is a central observation of this study, which we examine further in the following Sections.

It is helpful in understanding the consequences of the expulsion of interstitial brine from the mushy layer to compare and contrast the observations made using the present system with the results of previous studies in which there was no compositional convection. In a series of papers, Kerr *et al.* (1990*a*,*b*) developed mathematical models of binary alloys cooled from above which released a buoyant residual as they solidified. The residual liquid remained in the mushy layer and did not contribute to any convection. The models take account of heat conduction and latent heat release within the mushy layer and of the heat flux due to thermal convection in the liquid region. Kerr *et al.* (1990*a*, *b*) computed results in very close agreement with their experimental data, so we use the models here with confidence that any discrepancies between their predictions and our data are indicative of the influence of compositional convection.

In figure 7 we show the measured temperature of the liquid region as a function of

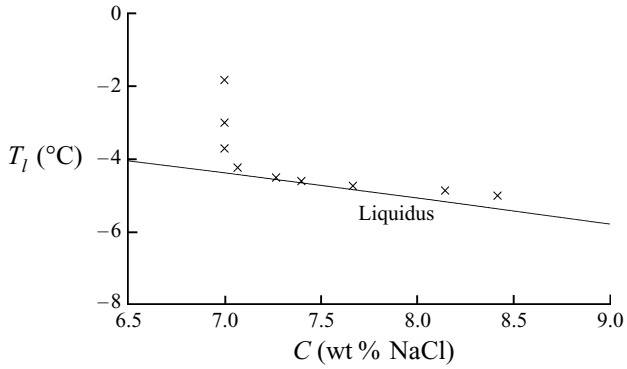

FIGURE 8. The trajectory of the temperature and concentration of the liquid region as they evolve in time. In the early stage of the experiment, thermal convection cools the liquid region to temperatures close to the liquidus temperature. Despite the small-scale compositional convection the composition of the liquid region remains almost constant. Once compositional convection from the interior of the mushy layer begins, the concentration of the liquid region increases. The continuing thermal convection keeps the temperature of the liquid close to the evolving liquidus temperature.

time and compare the data with four theoretical predictions. There are two parameters in the theory that may be influenced by the compositional field. One is a coefficient λ appearing in the relationship

$$Nu \equiv \frac{F_T(H-h)}{k(T_i - T_l)} = 2^{4/3}\lambda Ra^{1/3} \tag{3.1}$$

between the Nusselt number Nu for thermal convection in the liquid region and the Rayleigh number

$$Ra = \frac{(\rho_i - \rho_l)g(H-h)^3}{\mu\kappa}, \tag{3.2}$$

where F_T is the convective heat flux from the liquid region, T_i and ρ_i are the temperature and density of the liquid at the mush–liquid interface, T_l and ρ_l are the temperature and density of the fully liquid region, g is the acceleration due to gravity, $H-h$ is the depth of the liquid region, and μ, k and κ are the dynamic viscosity, thermal conductivity and thermal diffusivity of the liquid. The other parameter is a kinetic coefficient $\mathscr{G}$ which determines the degree of interfacial undercooling via the relationship

$$\dot{h} = \mathscr{G}\,[T_L(C_l) - T_i]\,, \tag{3.3}$$

where $T_L(C_l)$ is the liquidus temperature of the liquid region and the dot denotes differentiation with respect to time (Kerr *et al.* 1990*b*). Note that when the kinetic coefficient is large $T_i \approx T_L(C_l)$, which is the usual approximation of interfacial equilibrium. The first theoretical curve in figure 7 (shown with a short-dashed line) is the prediction made assuming interfacial equilibrium (effectively infinite kinetic coefficient $\mathscr{G}$) and the same value of λ (namely 0.056) used by Kerr *et al.* (1990*a*). As explained by Kerr *et al.* (1990*b*), interfacial undercooling can be significant, and they measured a value for $\mathscr{G}$ of 2.2×10^{-4} cm s^{-1} °C^{-1} for ice growing from a mixture of water and isopropanol. This same value of $\mathscr{G}$ is used in the prediction shown with a dash-dot curve in figure 7. It is possible to achieve a better fit to the data at early times by choosing a value of $\mathscr{G} = 4 \times 10^{-4}$ cm s^{-1} °C^{-1}, as shown by the solid curve in figure 7. A different value of $\mathscr{G}$ may be justified simply by

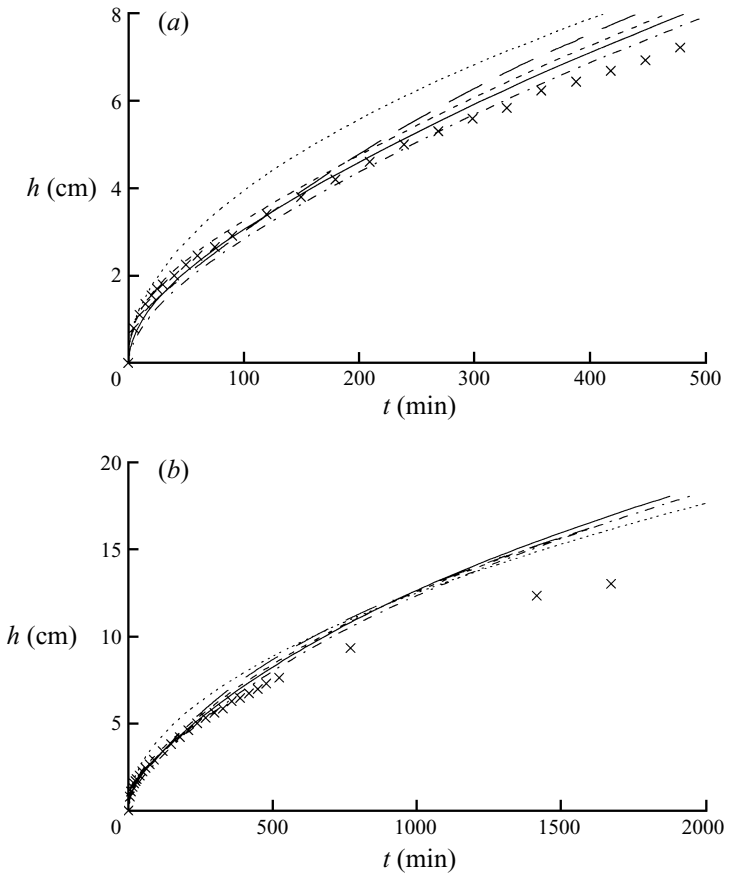

FIGURE 9. The depth of the mushy layer h as a function of time. The crosses show the experimental data while four of the curves show the predictions of a mathematical model with different values of the kinetic coefficient $\mathscr{G}$ and the heat-flux coefficient λ, as described in the caption to figure 7. The dotted curve shows the prediction of the theoretical model when thermal convection of the liquid region is neglected entirely.

the fact that we are working here with a different chemical system. The reason is that ice growing from pure water, parallel to the optical axis (perpendicular to the platelets), requires the nucleation of two-dimensional monomolecular height seeds for an undercooling between 0.03 and 0.3 °C (Wilen & Dash 1995). Furthermore, the nucleation barrier is sensitive to the nature of the impurities present in the melt (Wettlaufer 1997), so we expect different values of $\mathscr{G}$ for ionic impurities, such as NaCl, than for alcohol. A different value of $\mathscr{G}$ may also result from the fact that compositional convection reduces the contribution of constitutional supercooling to the interfacial undercooling by sweeping away excess solute. Good agreement with the data at early times can also be achieved by assuming interfacial equilibrium and increasing the value of λ to 0.12, as shown by the long-dashed curve in figure 7. A larger value of λ can be justified on the grounds that the compositional convection that augments the thermal convection is on a small scale that is influenced by the larger surface area presented by the tips of crystals at the mush–liquid interface.

It is clear that there are insufficient data to determine appropriate values of λ

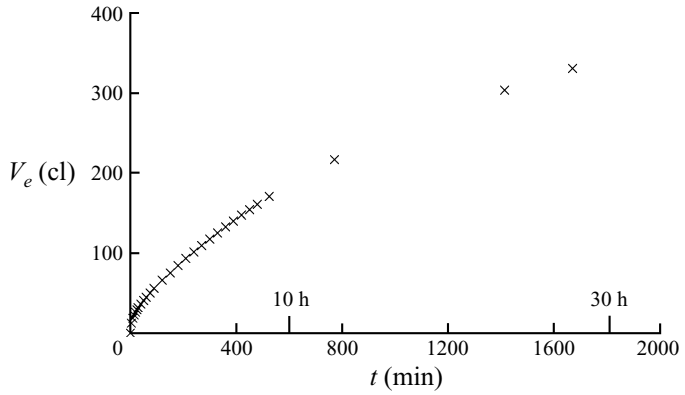

FIGURE 10. The volume of fluid V_e in the graduated burette (expansion tube) as a function of time during the experiment.

and $\mathscr{G}$ with any certainty in the present system. However, it is the nature of the disagreement between theory and experiment rather than any agreement that is of primary interest here. It is noticeable that none of the theoretical curves predict the steady decline in the temperature at late times. This contrast between theory and experiment highlights a consequence of compositional convection from the interior of the mushy layer. As the concentration of the liquid region increases (as shown in figure 6) its liquidus temperature decreases. In particular, the temperature at the mush–liquid interface decreases, which drives further thermal convection and cools the liquid region. Indeed, we see in figure 8 that the thermal convection is sufficiently strong to keep the liquid region close to its liquidus temperature as it evolves in time. This evolution of the concentration field is not taken into account in the theoretical predictions displayed in figure 7.

A further influence of the expelled brine can be deduced from figure 9, which shows the measured depth of the mushy layer as a function of time and four theoretical curves using the parameter values described above. Additionally, a theoretical prediction is shown in which the convective heat flux from the liquid region has artificially been set to zero. It is first worth noting that the range of values of λ and $\mathscr{G}$ used in trying to fit the temperature data makes little difference to the prediction of the growth of the mushy layer but that the thermal convection, though apparently weak, has a measureable influence on the growth. The mushy layer starts to grow more slowly than predicted by the theory after about 200 minutes. This is likely to be an indirect consequence of the brine expulsion which begins at about 200 minutes, as shown in figure 6. As we shall see below, the expulsion of brine causes the solid fraction of the mushy layer to increase. The associated increase in the amount of latent heat needed to be removed retards the growth of the mushy layer. The slower growth at late times may additionally be caused by some heat gains from the laboratory, which have a direct effect on thermal convection.

The last of the primary measurements made in our experiments was the volume of liquid in the expansion tube, shown as a function of time in figure 10. The expansion is due primarily to the increase in specific volume that occurs as water freezes to form ice. Roughly speaking, therefore, the volume of expansion V_e is proportional to the total volume of ice grown. However, great care is needed in order to interpret these data adequately, since V_e is also affected significantly by the change in the density of the liquid with both temperature T and concentration C and the change in the

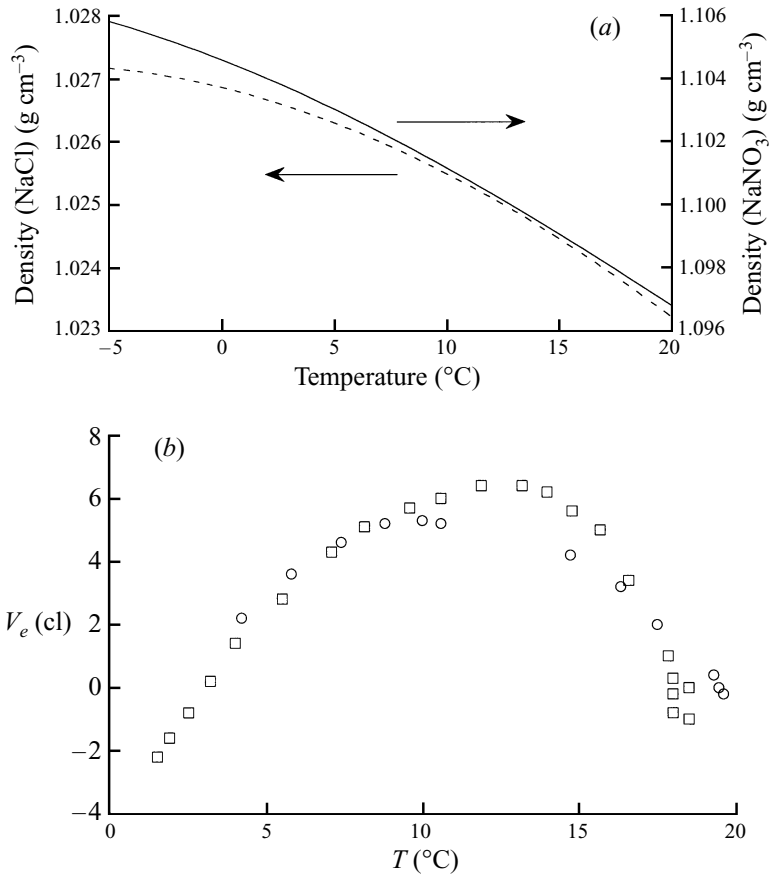

FIGURE 11 (a, b). For caption see facing page

volume of the experimental tank with temperature. Once these effects are taken into account, as described below, the measurements of the volume of expansion can be used to calculate the mean, vertically averaged, solid fraction in the mushy layer.

The liquid density as a function of temperature and concentration $\rho(T, C)$ was determined using a formula from Ruddick & Shirtcliffe (1979). The contraction of the tank was measured in additional experiments in which no ice was grown. Two different solutions were used (3.5% NaCl and 14% $NaNO_3$) with different thermal expansion properties, as shown in figure 11(a). Two experiments were performed with each solution: one in which the solution was cooled rapidly; the other in which time was allowed for the system to reach equilibrium after each new temperature was imposed. The results are shown in figures 11(b) and 11(c). If the tank were rigid then the volume of expansion V_e would be inversely proportional to the density of the liquid, which is monotonic for both the systems considered here over the temperature range investigated. It can be seen immediately that the relationship between the temperature and the volume of liquid in the expansion tube is non-monotonic in figure 11(b), and it can be verified that V_e is not inversely proportional to the density of the liquid for the data shown in figure 11(c). It is clear therefore that the variation of the volume of the tank with temperature has a significant effect on the volume of expansion V_e.

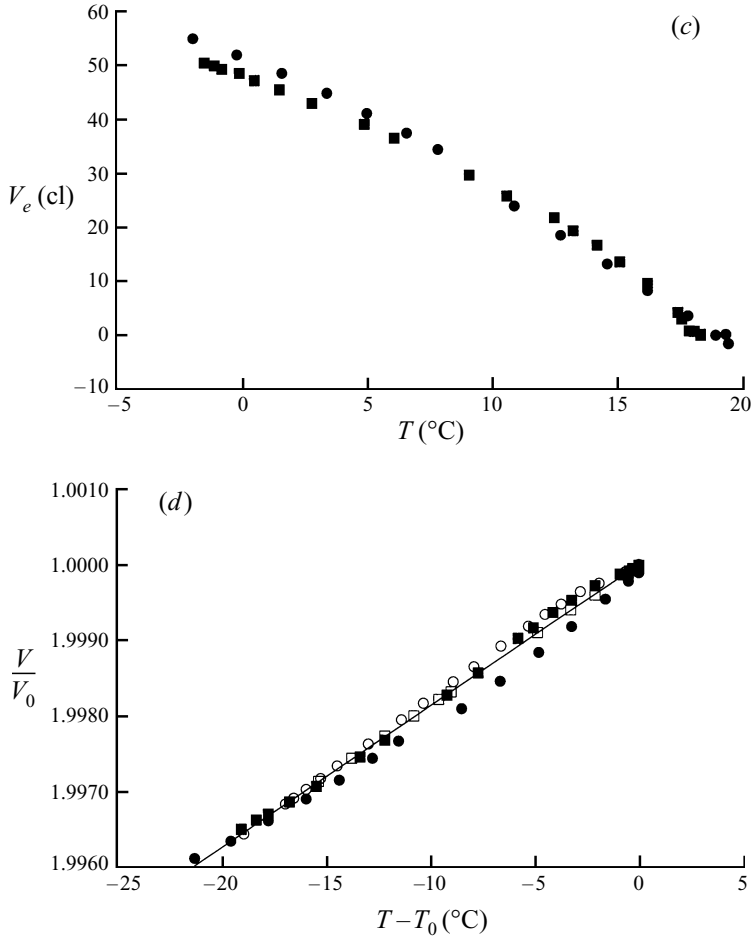

FIGURE 11. (*a*) The density of aqueous solutions of sodium nitrate (14 wt% $NaNO_3$) and sodium chloride (3.5 wt% NaCl) as functions of temperature. These solutions were used in additional experiments designed to determine the expansion properties of the experimental apparatus. The volume of fluid in the expansion tube is shown as a function of temperature during experiments in which (*b*) aqueous solutions of sodium chloride and (*c*) aqueous solutions of sodium nitrate were cooled without the formation of ice. The squares show the results obtained when the solutions were cooled rapidly. The circles show the results obtained when time was left for the apparatus to slowly relax to each new temperature. Part (*d*) shows the volume of the experimental tank relative to its initial value as a function of temperature. The line shows the best-fit linear relationship (3.5) through the data.

When no ice is grown, the volume of the tank $V(T)$ can be calculated by mass conservation, which gives

$$\frac{V(T)}{V_0} = \frac{\rho_0}{\rho(T)}\left(1 - \frac{V_e}{V_0}\right), \tag{3.4}$$

where $\rho(T)$ is the known density of the liquid as a function of its temperature T and ρ_0 and V_0 are the initial density of the liquid and volume of the tank respectively. In this formula, we have assumed that the liquid in the burette is at room temperature and hence retains its initial density. Since the burette contains only a small volume relative to the volume of the tank, any error in this approximation is correspondingly small.

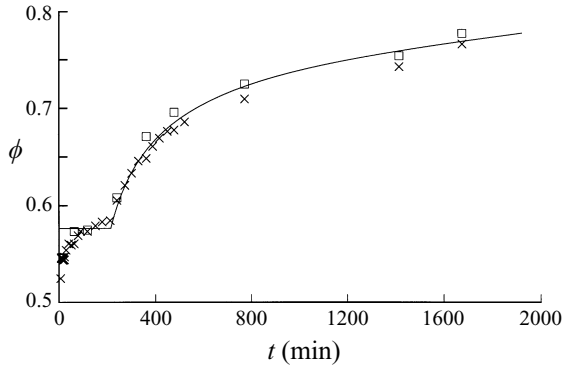

FIGURE 12. The mean solid fraction of the mushy layer as a function of time calculated from a mass balance (ϕ_m, equation (3.7), $\times$) and from a solute balance (ϕ_c, equation (3.9), $\square$). The solid curve is hand drawn to fit the data for ϕ_c.

Figure 11(d) shows that all four experiments give essentially the same relationship between the volume of the tank and the temperature, which is well approximated by the linear expression

$$V = V_0\,[1 - \gamma(T - T_0)]\,, \tag{3.5}$$

with $\gamma \approx 1.86 \times 10^{-4}\ ^{\circ}\mathrm{C}^{-1}$.

In the main experiments in which ice was grown, we estimate the mean, vertically averaged, solid fraction of the mushy layer as follows. We assume that the mushy layer has a solid fraction ϕ that is uniform with depth and that the solid phase has uniform density ρ_s. We estimate the density of the liquid in the mushy layer as $\rho_m = \rho(T_m, C_m)$, where $T_m = 0.5[T_L(C_l) + T_B] = T_L(C_m)$ and $T_L(C)$ is the liquidus temperature at concentration C (figure 2). Mass conservation for the whole system is expressed by

$$[\phi\rho_s + (1-\phi)\rho_m]hA_m + \rho_l[V(T) - hA_m] + \rho_e V_e = \rho_0 V_0, \tag{3.6}$$

which can be rearranged to give

$$\phi = \frac{\rho_e V_e + \rho_l V(T) - \rho_0 V_0 + (\rho_m - \rho_l)hA_m}{(\rho_m - \rho_s)hA_m} \equiv \phi_m, \tag{3.7}$$

where $\rho_l = \rho(T_l, C_l)$ and T_l and C_l are the measured values of the temperature and concentration of the liquid region. The mean solid fraction calculated from expression (3.7) is shown by the crosses in figure 12.

An alternative method for determining the mean solid fraction is via the equation

$$(1-\phi)\rho_m C_m hA_m + \rho_l C_l[V(T) - hA_m] + \rho_e C_e V_e = \rho_0 C_0 V_0, \tag{3.8}$$

expressing conservation of solute (cf. expressions given by Tait & Jaupart 1992 and by Huppert & Hallworth 1993). This equation can be rearranged to give

$$\phi = \frac{\rho_e C_e V_e + \rho_l C_l V - \rho_0 C_0 V_0 + (\rho_m C_m - \rho_l C_l)hA_m}{\rho_m C_m hA_m} \equiv \phi_c. \tag{3.9}$$

The value of the mean solid fraction estimated in this way is shown by the open squares in figure 12. The fact that the two estimates for ϕ agree shows consistency between the measurements of the volume of expansion and the measurements of concentration, and gives us confidence in the estimation of the solid fraction.

It should be noted that at early times both the numerator and denominator are small in expressions (3.7) and (3.9), which makes the calculation of solid fraction very sensitive to experimental error for those times. This is consistent with the fact that it is at early times that there is the greatest discrepancy between the two estimates of the mean solid fraction. It is tempting to conclude that the initial increase in ϕ_m, while ϕ_c is constant, is due to the nucleation barrier parallel to the horizontal c-axes causing disequilibrium in the interior of the mushy layer (Wettlaufer 1997; Wilen & Dash 1995). Such an effect would be seen in ϕ_m but, since it involves no transfer of solute out of the mushy layer, would not be seen in ϕ_c. Although we cannot be sufficiently confident in these early-time measurements to draw such a firm conclusion, for the reasons mentioned above, we believe that the idea warrants future study.

The data presented in figure 12 show that the solid fraction of the mushy layer increases monotonically with time. There is a sharp rise in the rate of increase after about 200 minutes at the same time when, as shown in figure 6(*a*), a significant salt flux out of the mushy layer commenced. We interpret this as indicating that as brine exits the mushy layer it is replenished by relatively fresh water from which more ice can be solidified.

4. Variations with external conditions

The experimental procedure described in the previous Sections was repeated for solutions of different initial concentrations C_0 and for different surface temperatures T_B. We begin here by showing the overall trends in the evolution of the system as these parameters vary.

Figure 13(*a*) shows how the depth of the mushy layer h grew as a function of time in three experiments in which the initial concentration C_0 was 7 wt% and T_B varied. As expected, we see that the growth is more rapid when the upper boundary is colder. We shall refer to the temperature difference $T_L(C_0) - T_B$ as the 'thermal driving' of the system. Greater thermal driving results in faster growth of the depth of the mushy layer.

Greater thermal driving (for a given concentration) also results in the mushy layer having a larger solid fraction, as shown in figure 13(*b*). This has a significant influence on the solute flux that can convect out of the mushy layer, since the greater solid fraction provides a greater resistance to the flow of interstitial liquid. For example, we see from figure 13(*c*) that the critical depth h_c before a significant solute flux began was largest in the experiment with the coldest surface temperature. This is a striking observation given that the compositional density difference across the mushy layer available to drive convection is greatest in this case. However, the greater resistance to flow associated with the larger solid fraction has the dominant influence and retards the release of interstitial brine.

Once the critical depth has been reached, the subsequent flux of solute was greatest in the system with the greatest thermal driving, as can be seen in figure 13(*d*). By this stage in the evolution of these experiments, the three systems had approximately the same solid fraction for a given depth of mushy layer (see §5), so the strength of the thermal driving alone determined the solute flux.

These trends are emphasized further in figure 14, where the evolutions of all experiments with the same value of the surface temperature $T_B = -20^\circ$C but different initial concentrations are shown. Since the liquidus temperature $T_L(C)$ decreases with concentration, the thermal driving $T_L(C_0) - T_B$ also decreases. The growth is therefore

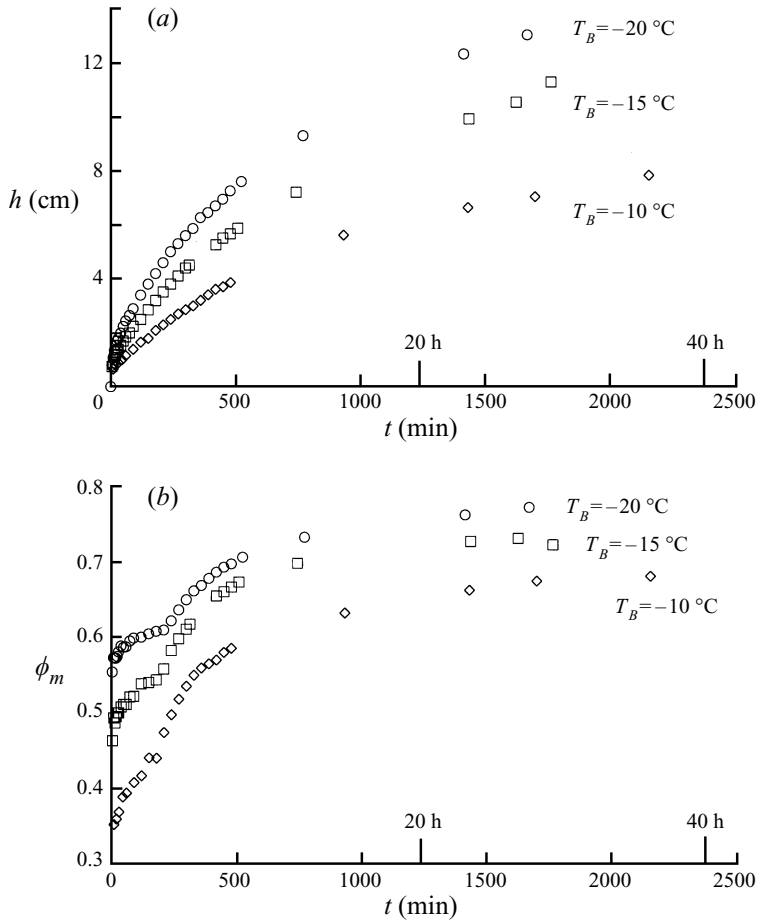

FIGURE 13 (*a*, *b*). For caption see facing page.

slower for larger values of C_0, as shown in figure 14(*a*) and the solid fraction is lower, as shown in figure 14(*b*).

In figure 14(*c*) we see again that the permeability has a greater influence on the release of solute from the mushy layer than does the thermal driving. At low initial concentrations the thermal driving is large but the solid fraction is also large so the resistance to flow is large. The latter effect is dominant and we see that the critical depth of the mushy layer decreases as the initial concentration increases.

Figure 14(*d*) shows that the solute flux increases as the initial concentration increases, even though the thermal driving decreases. This is in contrast with figure 13(*d*) which shows the solute flux increasing with the thermal driving. The results shown in figure 14(*d*) display the dominance of the solid fraction in determining the compositional convection since the solid fraction is large (the permeability is low) when the initial concentration is small.

We have seen qualitatively how the critical height h_c varies with the imposed conditions of the experiment. In the next Section we explore these variations quantitatively in an attempt to determine a general criterion for the abrupt onset of internally driven convection.

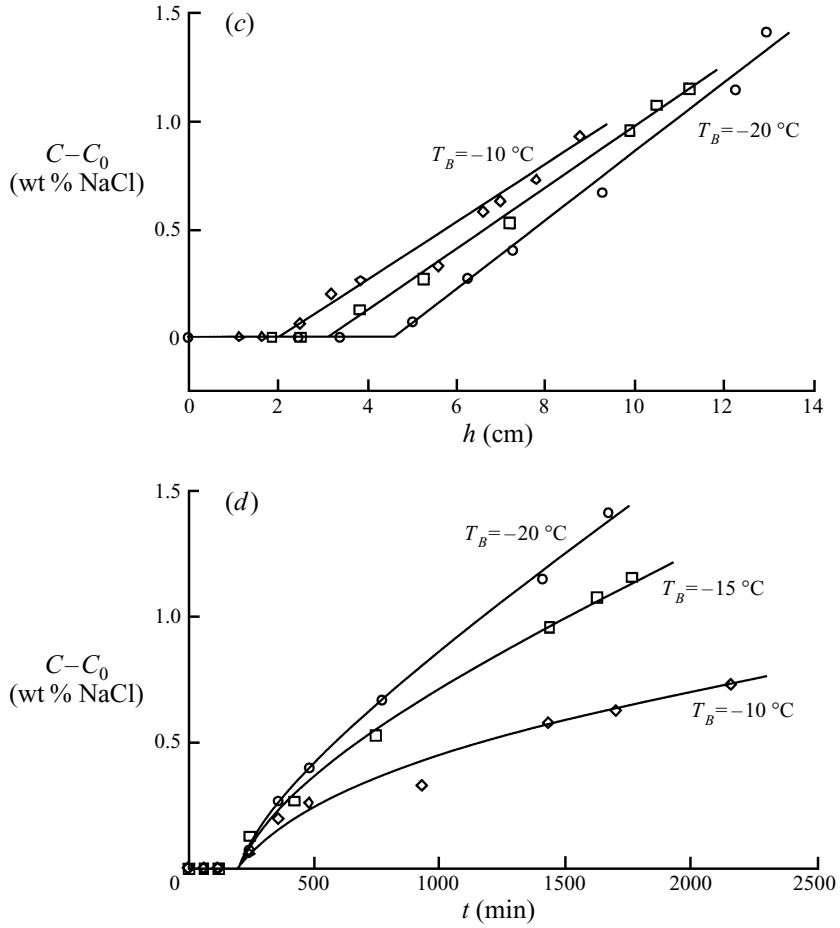

FIGURE 13. Data from three experiments with the same initial concentration ($C_0 = 7$ wt%) but different values of the surface temperature T_B. (*a*) The depth of the mushy layer as a function of time. (*b*) The solid fraction in the mushy layer as a function of time. (*c*) The concentration of the liquid region as a function of the depth of the mushy layer. (*d*) The concentration of the liquid region as a function of time. The fact that the onset of internally driven convection occurs at different stages in the evolution of a mushy layer is most clearly seen in (*c*).

5. The onset of compositional convection

We conducted a total of thirteen experiments as indicated in figure 2. For experiments with fixed initial concentration and different surface temperatures, the evolution of the solid fraction with time is displayed in figure 13(*b*). As discussed previously, there are two essential points conveyed in this plot. First, owing to the fact that, for fixed initial concentration, the mean temperature of the mushy layer decreases as the surface temperature decreases, the solid fraction at any time will be greater for experiments at lower values of T_B. Secondly, at a particular time in each experiment there is a distinct change in the slope of the curve. As was seen in figure 13(*c*), the value of h_c increases as T_B decreases, indicating that a critical mushy layer thickness is reached after which there is a release of solute into the bulk fluid, and a consequent increase in solid fraction.

We made a quantitative assessment of the conditions at the critical point as follows.

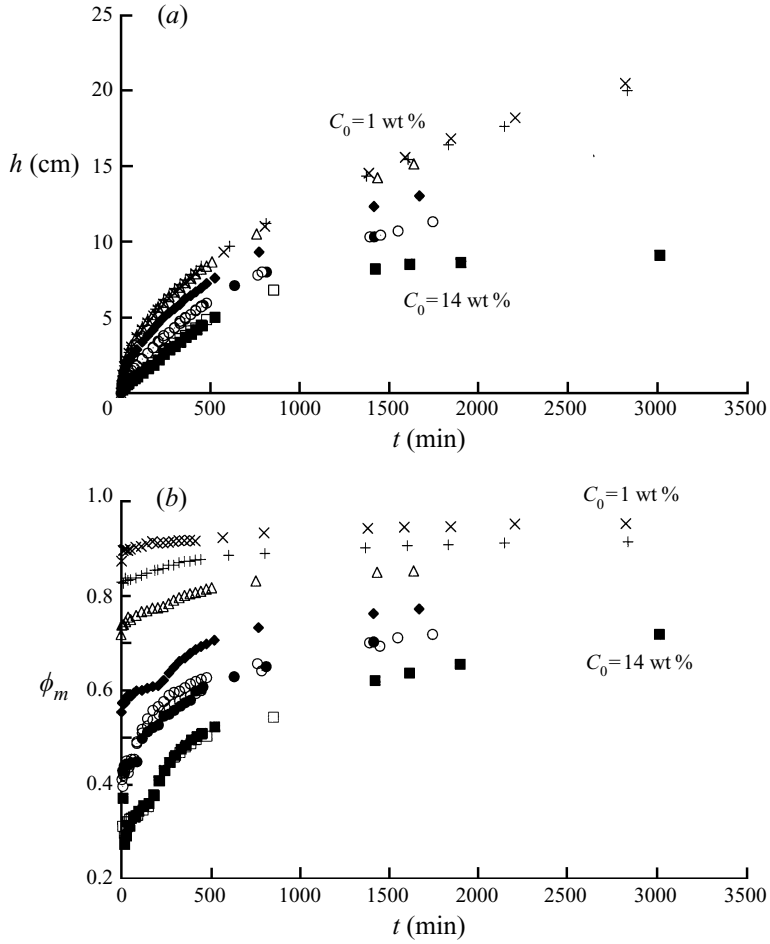

FIGURE 14 (*a*, *b*). For caption see facing page.

From graphs such as 13(*c*) we fitted a low-order polynomial (for $h(C)$) to the data corresponding to liquid concentrations greater than the initial concentration C_0, i.e. beyond the critical point. The polynomial was used to extrapolate backwards to determine the value of $h = h_c$, when $C = C_0$. The data for ϕ_m and h were then used to determine $\phi_{mc} = \phi_m(h_c)$, the value of the mean solid fraction at the critical point.

The critical height h_c varies considerably with the conditions of the experiment, T_B and C_0, as shown in figures 15(*a*) and 15(*b*). Although we can determine from these graphs the general trends that h_c increases as T_B decreases at fixed C_0 and that h_c decreases as C_0 increases at fixed T_B, the data generally display a striking lack of correlation. A reasonable collapse of all the data can, however, be achieved using the following physical hypothesis.

Theoretical stability analyses of growing mushy layers (Fowler 1985; Worster 1992*b*; Chen, Lu & Yang 1994) have shown that the buoyant interstitial fluid can remain motionless until a porous-medium Rayleigh number

$$Ra = \frac{g\beta\Delta C\Pi(\phi_m)h}{\kappa\nu} \tag{5.1}$$

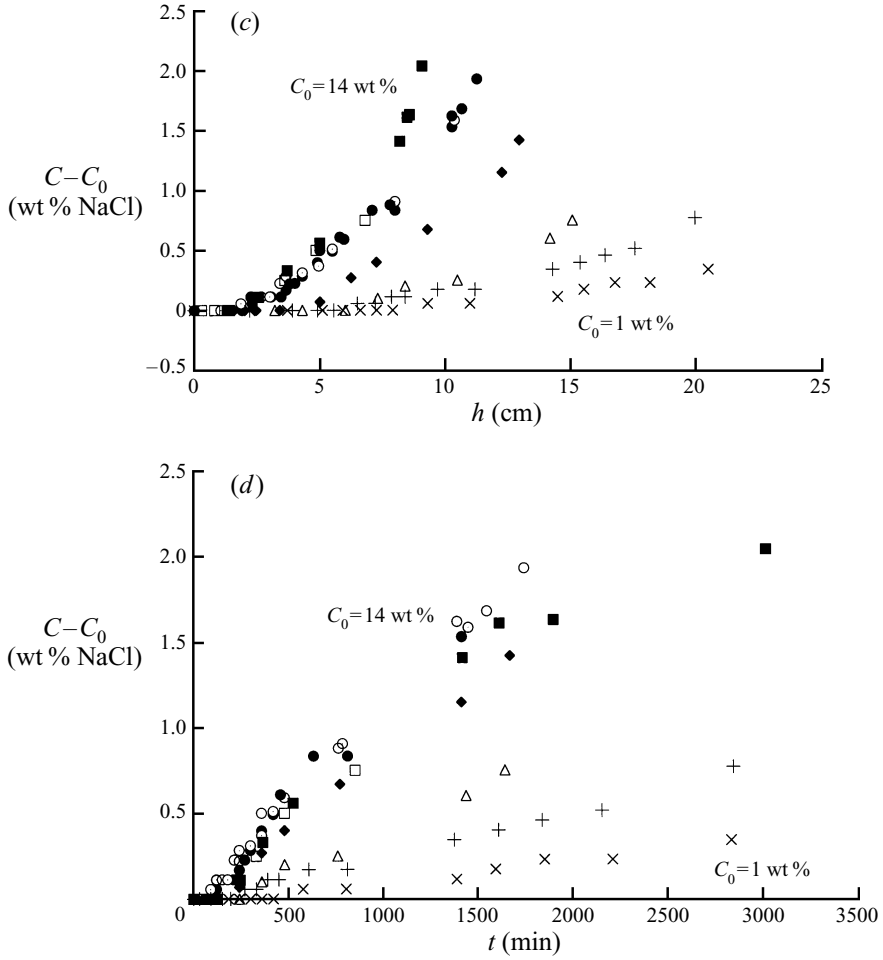

FIGURE 14. Data from nine experiments with the same surface temperature ($T_B = -20°C$) but different values of the initial concentration C_0: □, ■, two experiments with $C_0 = 14$ wt%; ○, ⊙, •, three experiments with $C_0 = 10.5$ wt%; ◆, $C_0 = 7$ wt%; △, $C_0 = 3.5$ wt%; +, $C_0 = 2$ wt%; ×, $C_0 = 1$ wt%. (*a*) The depth of the mushy layer as a function of time. (*b*) The solid fraction in the mushy layer as a function of time. (*c*) The concentration of the liquid region as a function of the depth of the mushy layer. (*d*) The concentration of the liquid region as a function of time.

exceeds a critical value Ra_c, where g is the acceleration due to gravity, $\beta\Delta C$ is the density contrast across the mushy layer proportional to the difference in liquid concentration $\Delta C = C_0 - C_B$, κ and ν are the thermal diffusivity and kinematic viscosity of the liquid and Π is the permeability of the mushy layer, which is a function of the solid fraction. Tait & Jaupart (1992) have, for example, shown experimentally that the critical height h_c is proportional to the kinematic viscosity ν of the liquid, which is consistent with this same hypothesis. Although the critical Rayleigh number depends somewhat on other dimensionless parameters of the system (Worster 1992*b*), here we make the assumption that the critical Rayleigh number is constant, which implies that

$$(h\Delta C)^{-1} \propto \Pi(\phi_{mc}). \tag{5.2}$$

In other words, $h\Delta C$ should be a function of ϕ_{mc} only, inversely proportional to the

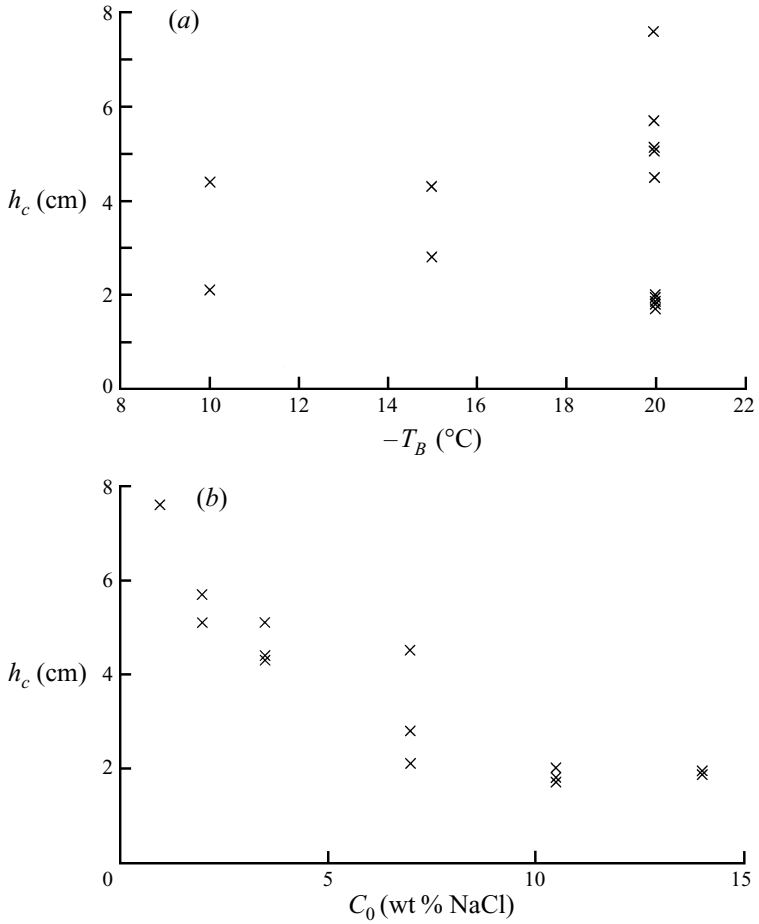

FIGURE 15. The critical depth of the mushy layer for all the experiments, shown in terms of the surface temperature T_B in (*a*) and in terms of the initial concentration in (*b*).

permeability of the mushy layer. In figure 16(*a*) we plot $h_c\Delta C$ against the critical solid fraction ϕ_{mc} for all the experiments. We observe that this provides a good collapse of all the data. Figure 16(*a*) can be treated as an empirical marginal stability curve. A mushy layer of thickness and solid fraction corresponding to the region below the curve is stable against solute release. In contrast, a mushy layer of thickness and solid fraction corresponding to the region above the curve is unstable to compositional convection leading to solute release and consequent evolution of the solid fraction. Additionally, looking at the data in a slightly different way in figure 16(*b*) we can see that the trend of the function is consistent with the expected form of the permeability function, namely that the permeability increases with the liquid fraction and has positive curvature, increasing rapidly at large values of the liquid fraction.

A number of cautionary points should be mentioned at this juncture. The method for estimating h_c relies on fitting the data of solute concentration as a function of the height of the mushy layer. Figure 14(*c*) clearly demonstrates that above a particular height there is an abrupt increase in the concentration of the bulk fluid. However, our ability to resolve the exact height at which the slope changes is limited by the temporal resolution of the solute data which itself depends on the initial concentration of a

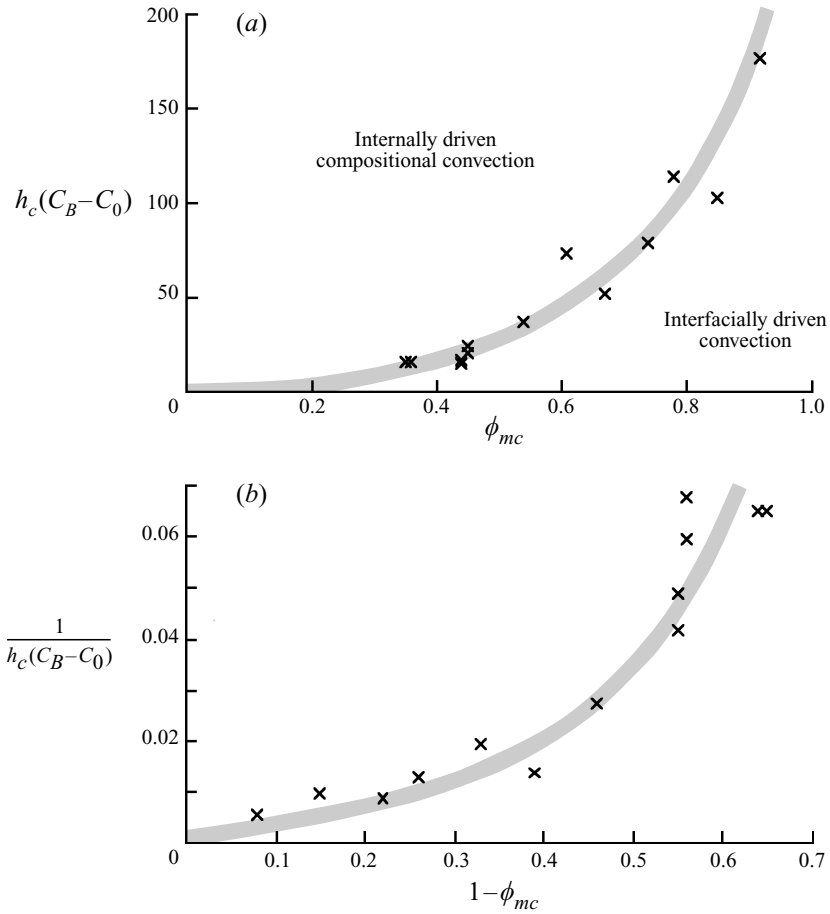

FIGURE 16. (*a*) The critical conditions for the onset of internally driven compositional convection. The crosses show the data for when the brine flux began in each experiment. When the conditions of the mushy layer lie below the marginal curve drawn through the data, most of the salt rejected by the growing ice remains trapped in the mushy layer. Once the conditions of the mushy layer lie above the marginal curve then brine is convected out of the mushy layer. (*b*) Here we display the same data in a different way by plotting $(h\Delta C)^{-1}$, which is proportional to the permeability, against the mean liquid fraction $(1-\phi_{mc})$. This shows that the trend of the observations is consistent with the expected form of the permeability function, namely that the permeability increases with the liquid fraction and has positive curvature, increasing rapidly at large values of the liquid fraction.

given experiment (i.e. for low initial concentrations, we are in a position of measuring small variations in a small quantity). We believe that the actual solute release begins at a height that is a little lower than that which we estimate. Furthermore, since we use h_c to estimate ϕ_{mc}, we believe that the critical value of the solid fraction is an upper bound. Therefore, the empirical marginal stability curve represents an upper bound for both $h_c\Delta C$ and ϕ_{mc}.

A final curiosity is shown in figure 17, where we plot the solid fraction as a function of the depth of the mushy layer for experiments with an initial concentration $C_0 = 7$ wt% and three different surface temperatures. It appears that once significant compositional convection from the mushy layer has begun (i.e. once the critical depth h_c has been exceeded) the data conform to a single curve. Similar results were found

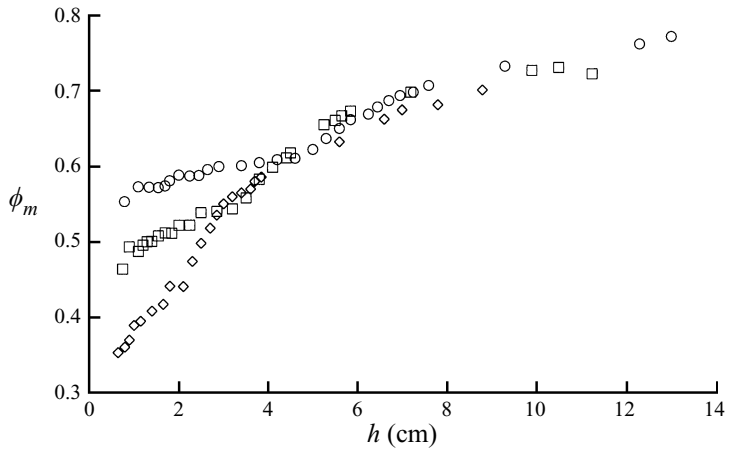

FIGURE 17. The mean solid fraction of the mushy layer as a function of its depth for three experiments with the same initial concentration ($C_0 = 7$ wt%) but different values of the surface temperature T_B. The data appear to collapse to a single curve once internally driven convection has begun.

for the experiments having $C_0 = 3.5$ wt%; the curves have a similar shape, but the solid fraction is generally higher. In other words, the solid fraction appears to be given by $\phi = \phi(h, C_0)$ independent of the surface temperature. The implication is that once $h > h_c$ in a given system, one need only know the depth of the mushy layer in order to determine its solid fraction. This observation merits further investigation.

6. Discussion and conclusions

We have conducted a systematic experimental study of the freezing of ice from salt water cooled from above. The ice forms a mushy layer whose interstices are filled with liquid enriched by the salt rejected by the growing ice. Although dense, the salty liquid remains within the mushy layer initially but, once the depth of the layer exceeds a critical value, compositional convection of brine into the underlying liquid region can commence.

The critical depth is larger when the surface temperature is colder for given initial concentration and is smaller when the initial concentration is larger for given surface temperature. In general, the critical depth is consistent with the hypothesis that it is determined by the critical conditions for compositional convection within the porous mushy layer.

The compositional convection out of the mushy layer allows fresher water to enter it, which promotes the further growth of ice within it and so increases the solid fraction. The present study provides the first laboratory measurements of the evolution of the solid fraction of sea ice. We have shown how the solid fraction increases with time, most markedly once the critical depth has been exceeded.

It is generally held that the brine flux from growing sea ice increases as the surface temperature decreases (gets colder). The accepted reason for this is simply that colder surface temperatures increase the rate of growth of ice and hence the rate of rejection of brine. However, as we have seen, the rejected brine can remain trapped within the mushy layer (sea-ice layer) and, indeed, that it remains trapped for longer and the critical depth is greater when the surface temperature is colder. Once the critical

depth is exceeded then the brine flux is indeed greater when the surface temperature is colder but this is because the contrast in the liquid concentration is then greater and provides a correspondingly greater density contrast to drive compositional convection.

We have found, in experiments with similar initial concentrations, that, once the critical depth has been exceeded, the solid fraction is a function of the depth of the mushy layer alone, independent of the surface temperature. Colder surface temperatures increase the rate of growth of the depth h of the mushy layer and also increase the rate of expulsion of brine thus increasing the rate of growth of the mean solid fraction ϕ, apparently in a way that keeps $\phi = \phi(h)$. We cannot yet offer an explanation for this but, if more generally true than within the constraints of our experimental procedure, this fact has extremely important implications. In particular, scattering theories developed specifically for the remote sensing of thin sea ice (Winebrenner *et al.* 1992) show that the volume scattering (as distinct from the surface scattering) is principally determined by the brine fraction (liquid fraction) of the ice. If indeed $\phi = \phi(h)$ alone then measurements of brine fraction would simultaneously determine the depth of the sea ice cover and hence the total solidified volume. This is a key observation for the monitoring of sea-ice climatology. Further implications of this work, including how our finding of an abrupt onset of brine flux affects the thermohaline structure in the Arctic Ocean, are discussed in Wettlaufer *et al.* (1997). It is possible that the overall brine flux is enhanced by the interaction between flow of the oceanic boundary layer and that within the sea ice. This is the subject of current study and has yet to be quantified.

It is our eventual goal to be able to construct a predictive theoretical model of the formation of sea ice. We have shown that existing models are adequate to make predictions in the early stages of its formation before a significant flux of brine from the mushy layer occurs. However, it remains to model the compositional convection within the mushy layer sufficiently to predict the salt flux once the critical conditions have been exceeded. The results of the experiments reported here should guide the development of future theories and provide a benchmark against which to test them.

We thank M. A. Hallworth for considerable help with the experiments and R. C. Kerr for useful comments on an earlier version of the manuscript. The work was partially supported by ONR N00014-94-1-0120, NSF OPP9523513 and NERC.

REFERENCES

Aagaard, K. & Carmack, E. 1994 A synthesis of Arctic Ocean circulation. In *The Polar Regions and Their Role in Shaping the Global Environment* (ed. O. M. Johannessen, R. D. Muench & J. E. Overland), pp. 5–20, Geophysical Monograph 85. American Geophysical Union.

Baines, W. D. & Turner, J. S. 1969 Turbulent buoyant convection from a source in a confined region. *J. Fluid Mech.* **37**, 51–80.

Bennington, K. O. 1963 Some crystal growth features of sea ice. *J. Glaciol.* **4**, 669–688.

Chen, C. F. & Chen, F. 1991 Experimental study of directional solidification of aqueous ammonium chloride solution. *J. Fluid Mech.* **227**, 567–586.

Chen, F., Lu, J. W. & Yand, T. L. 1994 Convective instability in ammonium chloride solution directionally solidified from below. *J. Fluid Mech.* **276** 163–187.

Copley, S. M., Giamei, A. F., Johnson, S. M. & Hornbecker, M. F. 1970 The origin of freckles in binary alloys. *Metall. Trans.* **A1**, 2193–2204.

Eide, L. I. & Martin, S. 1975 The formation of brine drainage features in young sea ice. *J. Glaciol.* **14**, 137–154.

Fowler, A. C. 1985 The formation of freckles in binary alloys. *IMA J. Appl. Maths* **35**, 159–174.

Gill, A. E. 1973 Circulation and bottom water production in the Weddell Sea. *Deep-Sea Res.* **20**, 111–140.

Hellawell, A., Sarazin, J. R. & Steube, R. S. 1993 Channel convection in partly solidified systems. *Phil. Trans. R. Soc. Lond.* A **345**, 507–544.

Huppert, H. E. 1990 The fluid dynamics of solidification. *J. Fluid Mech.* **212**, 209–240.

Huppert, H. E. & Hallworth, M. A. 1993 Solidification of NH_4Cl and NH_4Br from aqueous solutions contaminated by $CuSO_4$: the extinction of chimneys. *J. Cryst. Growth* **130**, 495–506.

Huppert, H. E. & Worster, M. G. 1985 Dynamic solidification of a binary melt. *Nature* **314**, 703–707.

Kerr, R. C., Woods, A. W., Worster, M. G. & Huppert, H. E. 1990*a* Solidification of an alloy cooled from above. Part 1. Equilibrium growth. *J. Fluid Mech.* **216**, 323–342.

Kerr, R. C., Woods, A. W., Worster, M. G. & Huppert, H. E. 1990*b* Solidification of an alloy cooled from above. Part 2. Non-equilibrium interfacial kinetics. *J. Fluid Mech.* **217**, 331–348.

Lake, R. A. & Lewis, E. L. 1970 Salt rejection by sea ice during growth. *J. Geophys. Res.* **75**, 583–597.

Morison, J., McPhee, M., Muench, R. *et al.*: THE LEADEX GROUP 1993 The LeadEx experiment. *Eos, Trans. AGU* **74**, 393–397.

Malmgren, F. 1927 On the properties of sea ice. In *The Norwegian Polar Expedition 'Maud,' 1918-1925, Scientific Results*, vol. 1a(5), pp. 1–67.

Peixoto, J. P. & Oort, A. H. 1992 *Physics of Climate*. American Institute of Physics.

Ruddick, B. R. & Shirtcliffe, T. G. L. 1979 Data for double-diffusers: physical properties of aqueous salt–sugar solutions. *Deep-Sea Res.* **26A**, 775–787.

Tait, S. & Jaupart, C. 1992 Compositional convection in a reactive crystalline mush and melt differentiation. *J. Geophys. Res.* **97**, 6735–6756.

Thorpe, S. A., Hutt, P. K. & Soulsby, R. 1969 The effect of horizontal gradients on thermohaline convection. *J. Fluid Mech.* **46**, 299–319.

Turner, J. S. 1979 *Buoyancy Effects in Fluids*. Cambridge University Press.

Weeks, W. F. 1997 Growth conditions and the structure and properties of sea ice. In *IAPSO Advanced Study Institute–Summer School: Physics of Ice–Covered Seas* (ed. M. Leppäranta). University of Helsinki.

Weeks, W. F. & Wettlaufer, J. S. 1996 Crystal orientations in floating ice sheets, In *The Johannes Weertman Symposium* (ed. R. J. Arsenault *et al.*), pp. 337–350. The Minerals, Metals & Materials Society.

Wettlaufer, J. S. 1997 Introduction to crystallization phenomena in sea ice. In *IAPSO Advanced Study Institute–Summer School: Physics of Ice–Covered Seas* (ed. M. Leppäranta). University of Helsinki.

Wettlaufer, J. S., Worster, M. G. & Huppert, H. E. 1997 The phase evolution of young sea ice. *Geophys. Res. Lett.* **23**, 1251–1254.

Wilen, L. A. & Dash, J. G. 1995 Giant facets at ice grain boundary grooves. *Science* **270**, 1184–1186.

Williams, K. L., Garrison, G. R. & Mourad, P. D. 1992 Experimental examination of growing and newly submerged sea ice including acoustic probing of the skeletal layer. *J. Acoust. Soc. Am.* **92**, 2075–2092.

Winebrenner, D. P., Bredow, J., Fung, A. K. *et al.* 1992 Microwave sea ice signature modeling. In *Microwave Remote Sensing of Sea Ice* (ed. F. Carsey), pp. 137–75. Geophysical Monograph 68, American Geophysical Union.

Worster, M. G. 1992*a* The dynamics of mushy layers. In *Interactive Dynamics of Convection and Solidification* (ed. S. H. Davis, H. E. Huppert, U. Müller & M. G. Worster). NATO ASI E219, pp. 113–138. Kluwer.

Worster, M. G. 1992*b* Instabilities of the liquid and mushy regions during solidification of alloys. *J. Fluid Mech.* **237**, 649–669.

Worster, M. G. & Kerr, R. C. 1994 The transient behaviour of alloys solidified from below prior to the formation of chimneys. *J. Fluid Mech.* **269**, 23–44.